JOURNAL OF SPACECRAFT AND ROCKETS
Vol. 29, No. 4, July–August 1992

Effects of g-Jitter and Marangoni Convection on Float Zones

N. Ramachandran*
Universities Space Research Association, Huntsville, Alabama 35812
and
C. A. Winter†
NASA Marshall Space Flight Center, Huntsville, Alabama 35812

The effects of g-jitter on three liquid zone experiments are numerically investigated. The g-level used in the study is composed of a steady component, characterizing the residual acceleration environment, and a time-varying component, characterizing the g-jitter environment. The time-varying component is comprised of either a sinusoidal or impulse disturbance. The response of both unencapsulated and encapsulated zone configurations are examined. The results indicate that complex flow patterns can arise that significantly modify the heat transfer characteristics of the system. The effects are more pronounced at the lowest frequency investigated (10^{-3} Hz), and impulsive accelerations imparted to fluids with large Prandtl numbers were found to have long decay times. Detailed velocity, temperature, average Nusselt number, and temperature sensitivity information are presented for many of the cases investigated.

Nomenclature

A,B	= g-jitter amplitude
Gr	= Grashof number, Ra/Pr
$\underline{g}$	= residual gravity
$\bar{g}$	= acceleration due to gravity
g_o	= terrestrial gravity, 981 cm/s^2
H	= height or thickness of float zone
h	= heat transfer coefficient
k	= thermal conductivity
L	= length of float zone; length scale
Ma	= Marangoni number
Nu	= average Nusselt number
Nu_o	= average Nusselt number, reference case
Nu_x	= local Nusselt number
P'	= pressure correction
Pr	= Prandtl number, ν/α
p	= pressure
Ra	= Rayleigh number, $g\beta\Delta TL^3/\nu\alpha$
T	= temperature
t	= time
U,V,W	= dimensionless Cartesian velocities ($/U_{ref}$)
U_{ref}	= velocity scale, $\lvert Ma\rvert\alpha/L$
u,v,w	= Cartesian (x,y,z) velocity components
X,Y,Z	= dimensionless Cartesian coordinates ($/L$)
x,y,z	= Cartesian coordinates
α	= thermal diffusivity
β	= thermal expansion coefficient
Δ	= difference
θ	= dimensionless temperature
μ	= dynamic viscosity
ν	= kinematic viscosity
ρ	= density
σ	= surface tension
τ	= dimensionless time, L/U_{ref}
τ'	= period of g-jitter, s
ψ	= stream function
ω	= g-jitter frequency, rad/s

Subscripts

ref	= reference quantity
1	= temperature suffix for hot disk
2	= temperature suffix for cold disk

Presented as Paper 90-0654 at the AIAA 28th Aerospace Sciences Meeting, Reno, NV, Jan. 8–11, 1990; received Feb. 5, 1990; revision received Nov. 7, 1991; accepted for publication Nov. 7, 1991.

*Associate Scientist. Member AIAA.
†Aerospace Engineer. Member AIAA.

Introduction

CRYSTAL growth methods have come into keen focus in recent years as the capabilities of obtaining larger and higher quality crystals are investigated in a low-gravity environment. Several crystal growth related experiments have been performed during previous extended space missions, and more opportunities are anticipated in future space flights. The floating zone crystal growth method, which is often used in the ground-based production of semiconductor crystals, may prove to be an attractive method for space operations.

A reduction in gravity, while tending to minimize buoyancy-driven convection, also results in the reduction of the hydrostatic pressure. Such a reduction in pressure prevents liquid in a floating zone configuration from deforming under its own weight and allows longer, more stable zones to be formed. From these zones, larger crystals can be solidified. Further, the float zone geometry is a partially containerless system, being that the circumferential surface is almost entirely in contact with the fluid surrounding it except at the solidus walls. Such containerless processing eliminates wall effects such as contamination and nucleation at the cylindrical zone wall and allows the formation of more pure and perfect crystals. In addition, the absence of the ampoule wall allows unconstrained material expansion during freezing, preventing sample breakage and other constrainment effects.

The floating zone configuration, while beneficial in reducing wall effects, may experience a second type of convection, initiated and sustained by thermal or solutal gradients along the zone free surface. This convection, now related to surface tension rather than gravitational forces, is called Marangoni convection and results because fluid elements on the free surface with a low surface tension tend to flow to fluid areas of higher surface tension. Because the float zone process is one in which a material is melted and then resolidified, axial and longitudinal thermal and solutal gradients are sure to exist within the zone, acting as drivers for this convective flow. Such Marangoni convection may produce oscillatory tempera-

tional homogeneity of the processed crystal. In the space environment, Marangoni convection is expected to be the dominant force in a float zone melt. Some of the deleterious effects of buoyancy and Marangoni convection can be reduced by crystal rotation, an operation that tends to stabilize any present oscillatory thermal/solutal fields. In addition, a further reduction of the Marangoni effect may be achieved by encapsulation (or coating) of the zone, a process that tends to reduce the surface tension flow at the free surface. Experimental research involving float zone silicon melts reported by Eyer et al.[1] indicated that surface tension driven convection is the predominant driving force both on Earth and in low gravity, as both terrestrial and Spacelab 1 crystals had similar striation patterns. Further, Earth-grown silicon crystals that were coated with silica to suppress Marangoni convection were shown to be striation free.[2] Experiments by Croell et al.[3,4] also demonstrated a reduction of Marangoni convection via melt coating. A silicon sample coated with a 5-μm-thick SiO_2 film was melted and solidified during the low-gravity sounding rocket flight. The dopant boron, applied to the edge of the crystal, was released during melting to map either the diffusive or convective behavior of the melt. It was reported that a purely diffusive character was observed in the flight sample, whereas laminar convection was observed in the corresponding ground sample. Float zone encapsulation of gallium arsenide (GaAs) crystals with boron trioxide has been studied by Barocela and Jalilevand.[5] Reportedly, such encapsulation will prove to have several advantages, including the suppression of Marangoni convection and the reduction of evaporation of compounds during growth. Further, these semiconductors, employed for both electronic and light emitting diodes, are prime candidates for low-gravity materials processing.

Acceleration Environment

During past space investigations, many experiments have been suspected to have been affected by the imposed acceleration environment. There are few experiments, however, that correlated the sensitivity of the fluids experiment to the measured-time-dependent low-gravity disturbances. Therefore, efforts are being made to determine the acceleration effects and possibly reduce the disturbances experienced by the fluid system. For example, if fluid sensitivity can be characterized in a computational, quantitative way, vibration isolation systems might be tuned to filter bandwidths expected to produce adverse effects.

Because of the importance attributed to gravity forces that drive the fluid, calculations described herein represent resultant flowfields produced as quasisteady, oscillatory, and/or transient acceleration forcing functions are applied. Realistic acceleration inputs were sought for the calculations, and estimations of spacecraft accelerations were researched. Magnitudes and/or frequencies of suspected spacecraft accelerations discussed here have been presented by Ostrach,[6] Demel,[7] and Hammacher.[8]

Spacecraft drag and gravity gradient effects contribute to the quasisteady acceleration that impacts experiments within the vehicle. These accelerations are dependent on vehicle altitude and attitude, as well as position within the vehicle, and are expected to produce very small but steady disturbances in the range of 2.0×10^{-8} to $6.0 \times 10^{-6} g_o$. Such disturbances include very low frequencies corresponding to the orbital period of the spacecraft. These accelerations in the orbital regime were cited having frequencies of 1.0×10^{-6} to 5.0×10^{-3} Hz.[7]

Transient accelerations (attributed to crew motion, spacecraft attitude control maneuvers, etc.) and oscillatory motions (attributed to rotating machinery, etc.) are expected to typically produce somewhat larger disturbances in the range of 3.0×10^{-6} to $4.2 \times 10^{-4} g_o$. These accelerations were cited as having frequencies from 5.0×10^{-3} to over 100 Hz. More specifically, Ostrach[6] notes that crew motion throughout the mission will most likely be random in nature, distributed over a frequency range from 0.1 to 10 Hz and having a peak amplitude at 1 Hz. Amplitudes associated with this motion are expected to be $3.0 \times 10^{-5} g_o$ when the crew is asleep and, of course, much higher during full duty hours. Transient accelerations measuring as high as $1.0 \times 10^{-2} g_o$ were observed on the German Spacelab D1[8] and during Spacelab 3.

The previously mentioned quasisteady and g-jitter accelerations not only affect the onset and development of convective motion in the float zones due to buoyancy forces, but also have an impact on the stability of the zone itself. During the silicone oil bridge experiments on Spacelab D1,[9,10] column breakage occurred a total of six times, twice specifically attributed to g-jitter effects and other times related to mechanically imposed axial oscillations. Although it is expected that higher frequencies, greater than 0.1 Hz, can be isolated by the use of passive or active isolation techniques, lower, possibly critical frequencies will still be imposed on the experiments. The effect of these disturbances on the flow and heat transfer in the float zones has yet to be fully understood.

Questions then arise as to the practicality of vibration isolation systems for certain classes of experiments. If experiments are most sensitive to accelerations in the critical region where isolation systems can function effectively, is the cost of implementing such a system feasible? To what levels should the isolation bandwidths be chosen for each different experiment scenario? Will isolation systems be highly practical for impulsive type disturbances, but ineffective for very low frequency accelerations? To answer such questions, the sensitivity of fluids experiments to low gravity disturbances must be examined.

Choosing an Experiment Class

A review of fluids and materials processing experiments[11] that were performed in the low-gravity environment was completed, and experiments expected to be particularly sensitive to a vibration environment were considered for analysis. It was noted that over 50 separate investigations had been initiated to study thermocapillary or liquid zone stability fluid characteristics. Because the sensitivity of each fluid system could not be examined, thermocapillary, liquid bridge, and float zone space experiments were reviewed and typical experimental parameters were noted. Fluid parameters for each experiment setup were uniquely different. Liquid choices and corresponding Prandtl numbers of the experiments were examined as a range of fluid sensitivities were sought.

The silicone oil experiment of Napolitano,[12] performed during the German Spacelab Mission D1, was chosen for analysis. The Prandtl number associated with this research was 60. The experiments examined the Marangoni convection resulting in one and two liquid bridges. Reportedly, a single fluid, 6-cm silicone oil liquid bridge was created exhibiting a "purely cylindrical shape." Heating of the feeding disk to 60°C induced Marangoni flow, but its nature was not oscillatory. The silicon melt ($Pr = 0.023$) experiments of Eyer et al.[1] (briefly described in an earlier section) examined the floating zone production of the phosphorous-doped silicon system during Spacelab 1 (and TEXUS 7) and were also chosen for analysis. Having chosen two practical experiments whose Prandtl numbers were 60 and 0.023, a third experiment was sought that had a Prandtl number between these two values. The liquid bridge experiments of Chun[13] performed during experiments aboard the German TEXUS sounding rocket program were chosen for this purpose.

Analysis Goals

The aim of this investigation was twofold: 1) to examine the convective fluid dynamics resulting from quasisteady and g-jitter accelerations on float zone and liquid bridge experiments, and 2) to begin to quantify the acceptable g-tolerance levels of these systems.

Fluid characteristics and system parameters of the selected space investigations (Table 1) were implemented into analysis.

Computations examined the overall buoyancy-driven and surface-tension-driven convective flows within the zone rather than the intricacies of the crystal growth at the interface. Such analysis provides much information about the diffusive nature of the fluid and the thermal distribution of the flow in the critical area around the crystalline interface. Thus, highly detailed modeling of each fluid class was not the objective, rather determination of the overall fluid response to imposed gravitational disturbances was the goal. It should be noted that solutal contributions were not input into the computations as presented here.

Physical Setup and Governing Equations

A schematic illustrating the computational float zone geometry, residual gravity vector, and imposed g-jitter profile is shown in Fig. 1. The two-dimensional, horizontal floating zone, is simulated in a Cartesian coordinate system as a liquid bridge suspended between two solid walls. A thermal gradient is imposed across the bridge by maintaining the left-hand wall at a hot temperature T_1 and the right-hand wall at a cold temperature T_2. The free surfaces of the zone are assumed flat, nondeformable, and thermally adiabatic. The imposed g-level is comprised of a mean value or quasisteady acceleration $\bar{g}$ and a time-varying g-jitter component. The g-jitter component consists of either a sinusoidal disturbance with amplitude A and frequency ω, or an impulsive disturbance of amplitude B and a duration of 1 s. All gravity components are applied perpendicular to the temperature gradient. The equations and boundary conditions governing the simulation are presented in Eqs. (1–8). An incompressible, Newtonian-Boussinesq fluid exhibiting laminar flow is assumed. All fluid properties (except for the fluid density) are chosen to be constant.

Continuity:

$$u_x + v_y = 0 \tag{1}$$

Momentum:

$$u_t + uu_x + vu_y = -p_x/\rho + \nu(u_{xx} + u_{yy}) \tag{2}$$

$$v_t + uv_x + vv_y = -p_y/\rho + \nu(v_{xx} + v_{yy}) + g\beta(T - T_{\text{ref}}) \tag{3}$$

Energy:

$$T_t + uT_x + vT_y = \alpha(T_{xx} + T_{yy}) \tag{4}$$

Boundary conditions:

walls

$$u = v = 0 \qquad \text{at} \qquad x = 0,\ x = L \tag{5}$$

free surfaces

$$\mu\, u_y = \sigma_T\, T_x \qquad \text{at} \qquad y = 0,\ y = H \tag{6}$$

hot side

$$T = T_1; \qquad x = 0$$

cold side

$$T = T_2; \qquad x = L \tag{7}$$

Table 1 Float zone parameters and properties

Fluid	Silicone oil	Methanol	Silicon melt
Flight	D-1, 1986[12]	TEXUS-7, 1984[13]	Spacelab-1, 1984[1]
Pr	60	6.827	0.023
L, cm	6.0	1.0	2.0
ΔT, K	32	10	50
σ_T, d/cm.K	-0.0655	-0.0773	-0.43
μ, g/cm.s	4.56×10^{-2}	5.84×10^{-3}	7.5×10^{-3}
ρ, g/cm^3	0.91	0.792	2.50
ν, cm^2/s	5.01×10^{-2}	7.374×10^{-3}	3.0×10^{-3}
α, cm^2/s	8.40×10^{-4}	1.08×10^{-3}	0.13
β_T, 1/K	1.05×10^{-3}	1.19×10^{-3}	1.43×10^{-4}
Gr, 1 g_o	2.66×10^6	2.147×10^5	6.235×10^6
Ma	-2.97×10^5	-1.226×10^5	-4.41×10^4

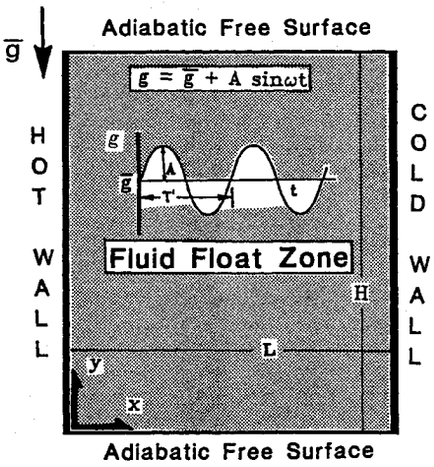

Fig. 1 Schematic of the setup and the g-jitter profile.

$$T_y = 0; \qquad \text{at} \qquad y = 0,\ y = H \tag{8}$$

In Eqs (1–8), a subscript denotes partial differentiation of the variable with respect to that subscript. Equation (6) balances surface tension and shear forces at the free surfaces. Representing the fluid gradient of surface tension with temperature, σ_T decreases linearly with temperature for the three liquids considered in this study. Hence, σ_T is negative in all proposed computations.

The equations and boundary conditions are placed into dimensionless form using L as the reference length, U_{ref} as the reference velocity, and (ΔT) as the temperature scale. Ma is defined as

$$Ma = \sigma_T \Delta T L/(\mu\alpha) \tag{9}$$

Based on these reference quantities, the resultant flow and thermal fields are given in terms of the dimensionless stream function and temperature

$$U = \psi_Y, \qquad V = -\psi_X, \qquad \theta = (T - T_2)/(T_1 - T_2) \tag{10}$$

Using the scaling factors, boundary condition (6) becomes

$$U_Y = -\theta_X \tag{11}$$

The time scale for the transient computations is determined from the ratio of the reference length to the reference velocity. In computations that consider a quasisteady acceleration ($\bar{g}$) coupled with a sinusoidal disturbance, the g is written in Eq. (3) as

$$g = \bar{g} + A\,\sin(2\pi\omega t/\tau') \tag{12}$$

where ω is the g-jitter frequency and τ' is the period of oscillation.

Numerical Method

The governing equations and boundary conditions are solved in the primitive variables using an implicit control volume based finite difference method similar to the one proposed by Gosman et al.[14] The discretized equations are solved iteratively using the SIMPLE-C pressure-velocity correction algorithm.[15,16] The code utilizes central differencing for the spatial discretization of the diffusion terms and positive coefficient skew upwind differencing for the convective terms. An iterative procedure using the alternating direction implicit (ADI) scheme is used for global iterations among the equations. Convergence is obtained when the following criterion is satisfied after successive iterations of the equations.

$$\text{Error} = (|\Delta U|_{\max} + |\Delta V|_{\max})/U_{\text{ref}} + |P'|_{\max}/(\rho U_{\text{ref}}^2) + (|\Delta T|_{\max}/T_{\text{ref}}) \le 10^{-4} \tag{13}$$

where the terms on the right-hand side are the computed residuals in the momentum equations, the Poisson equation for pressure, and the energy equation, respectively.

All the computations were done for a unit aspect ratio zone (H/L = 1). A 31 × 31 staggered orthogonal grid was used for $Pr = 0.023$ and 6.827. A 41 × 41 staggered grid was employed for $Pr = 60$, as preliminary calculations showed the inadequacy of a 31 × 31 grid to sufficiently resolve the thermal boundary layer for this Prandtl number. In addition, different time steps were examined to ensure that the chosen time step was adequately small. Computational analysis of the floating zone configuration was first examined with only surface tension driven forces contributing to the convective motion. Once steady-state solutions of these pure Marangoni computations were realized, the resultant flow and thermal fields were used as the starting conditions for the transient computations. In these subsequent calculations, both Ma and gravity-driven effects were examined. The local and average Nusselt numbers are used to present the system heat transfer characteristics. These quantities are defined as follows:

Local Nusselt number:

$$Nu_x = hL/k = -\theta_X \tag{14}$$

Average Nusselt number:

$$Nu = \frac{1}{H}\int_0^H Nu_x \, dy \tag{15}$$

Acceleration magnitudes and frequencies typical of those that might be encountered on the Shuttle or Space Station (10^{-3}–0.1 Hz) were imposed over the fluid systems. Practical vibration isolation limits are near the 0.1-Hz frequency cutoff; thus, the computations consider realistic vibration isolation disturbance filtering limits and examine fluid response at and below these limits.

Results and Discussion

Computations were completed for both unencapsulated and encapsulated zones for the three chosen experiments. In all of the subsequent discussions, the steady-state results used as initial conditions for the time-accurate computations will be referred to as the reference case and the corresponding average Nusselt number will be denoted as Nu_o.

Unencapsulated Float Zones

Using fluid properties, as presented in Table 1, the steady-state solutions for the three fluids subjected to surface-tension-driven convection alone are shown in Figs. 2. The Marangoni numbers used in the computations are -10^5, -1.2×10^5, and -10^4 for $Pr = 60$, 6.827, and 0.023, respectively. The maximum and minimum values of the stream function and the Nu_o values for each case are also indicated in the figures. In all of the three cases, vigorous convection in the zone sets up two symmetric counter-rotating cells. The calculations indicate that the maximum velocities on the free surfaces are located adjacent to the cold wall for all three cases. These velocities are 4.43 cm/s for silicone oil, 39.39 cm/s for methanol, and 145.4 cm/s for the silicon melt. The average surface velocities, however, are much smaller than these maximum values: approximately 0.33, 2.23, and 8.32 cm/s for $Pr = 60$, 6.827, and 0.023, respectively. These strong circulations result in significant distortion of the isotherms. The enhanced heat transfer is evidenced by the large values for the average Nusselt numbers. In all of the cases, the Marangoni driven flow was steady and no difficulties were encountered in obtaining a converged solution. Flight experiments with the methanol bridge[13] experienced flowfield oscillations that were attributed primarily to Marangoni forces. However, the observed unsteady flow behavior is not reproduced by the two-dimensional computations.

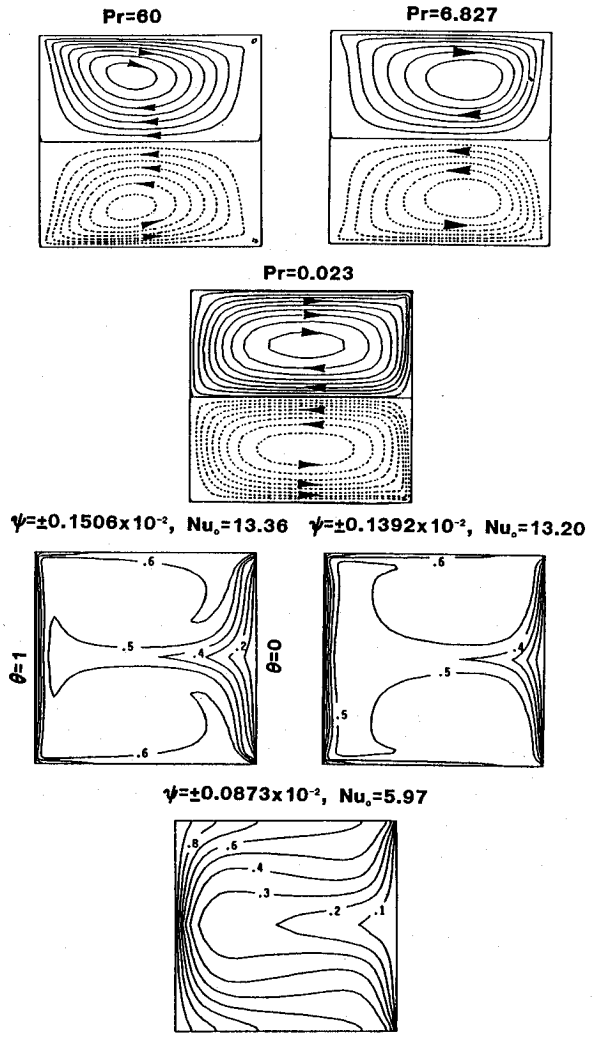

Fig. 2 Stream function and isotherm distributions; pure Marangoni convection; $\Delta\psi = 2 \times 10^{-4}$.

In order to gauge the effect of residual and g-jitter accelerations on these strong, Marangoni flows, the steady-state results were used as initial conditions for subsequent computations. A constant, residual gravity level of $10^{-5} g_o$ was chosen and coupled with a time-varying sinusoidal disturbance of amplitude $10^{-3} g_o$ and frequency of 10^{-2} Hz. Time-accurate solutions were computed over five periods of g-jitter for each case.

The stream function and isotherm distributions over one complete cycle of g-jitter are shown in Figs. 3 for $Pr = 60$. The silicone oil bridge has already been subjected to four periods of g-jitter forcing. Comparing resultant flow and thermal fields for $Pr = 60$ (Figs. 2 and 3), it is observed that gravity contributions do induce some effects; for example, the two cells in the flowfield wax and wane, alternately, in step with the frequency, whereas the isotherm response shows a phase lag of $\pi/2$. Figure 4 shows the plot of the maximum temperature change experienced at any point within the zone and the maximum velocity changes (compared to the reference case) on the top and bottom free surfaces during five cycles of computation. The figure indicates that periodic behavior of the thermal field is attained after one cycle, whereas the periodic behavior of the flowfield is achieved after approximately two cycles. The maximum increase in velocity along the free surface is 70% larger than that for the reference pure Marangoni case, and the maximum change in temperature within the zone is around 5 K. This represents a change in the average surface velocity from 0.32 cm/s (reference case) to 0.54 cm/s.

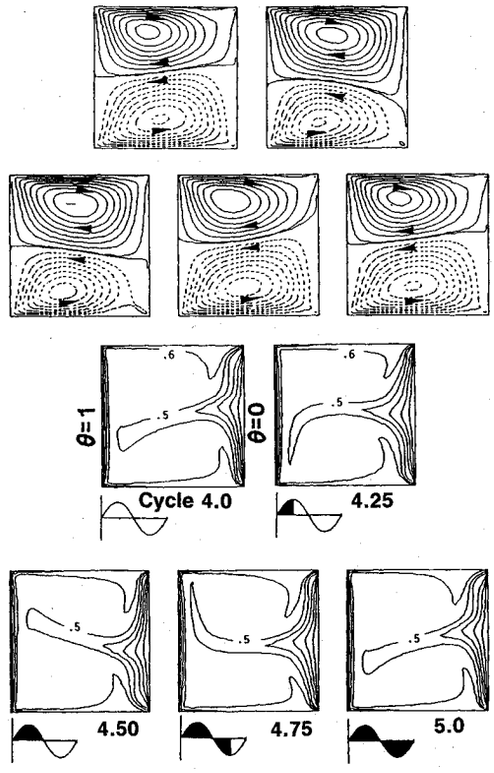

Fig. 3 Stream function and isotherm distributions: $\omega = 10^{-2}$ Hz, $Pr = 60$, $Ma = -10^5$.

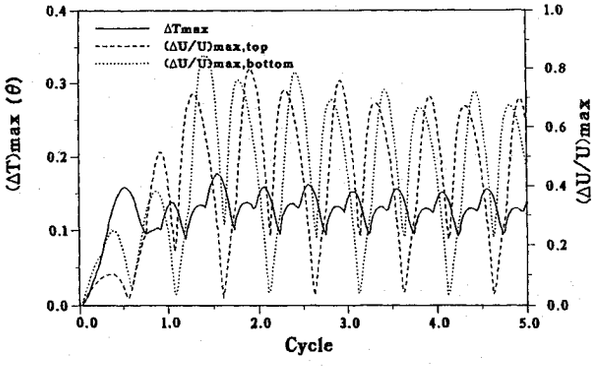

Fig. 4 Temperature and velocity changes due to g-jitter: $\omega = 10^{-2}$ Hz, $Pr = 60$, $Ma = -10^5$.

Calculations for $Pr = 6.827$ and 0.023 illustrated that residual and g-jitter contributions on the flow and thermal fields were less detrimental than for $Pr = 60$. For the Si melt, the maximum velocity change at the free surface is about 0.08% and the maximum temperature change in the zone is ≈ 0.02 K. The resulting overall Nu variation over the corresponding reference case is -0.015%. Similarly, for the methanol zone, the temperature change is 0.002 K, the Nu change is -0.08%, and the velocity variation is $\approx 0.35\%$. The imposed gravity effects on these two cases are, thus, significantly reduced.

For other frequencies ($\omega > 10^{-2}$ Hz), g-jitter computations revealed negligible effects on the induced velocity and temperature fields; thus, the results for these cases are not presented here. It suffices to say that, in flows dominated by Marangoni convection, the g-jitter modifications are, if anything, very minor in nature. For large Pr fluids, these effects are more prominent than for small Pr fluids. It should be emphasized that, although no large g-jitter impact was noticed in the zone thermodynamic behavior, the large surface tension induced velocities can impact the stability and shape of the zone and this factor is of considerable concern for the successful completion of an experiment.

Encapsulated Float Zones

Results are now presented for the encapsulated float zone geometry for the same three fluids considered in the previous discussions. Sixteen different transient cases were simulated and are tabulated in Table 2. The residual, or quasisteady g force was imposed on all 16 cases. A value of $10^{-5} g_o$ was selected for this parameter, representing a worst-case scenario. The g-jitter force coupled to this residual g force was represented by either a sinusoidal wave form (cases 1-3, 6-9, 12-14), or an impulsive input (cases 4, 5, 10, 11, 15, and 16). The amplitude A of the imposed sinusoidal wave form ($A \sin \omega t$) was always chosen as $10^{-3} g_o$, again representing a worst-case scenario.

Although it is known that liquid encapsulation significantly reduces the surface-tension-driven convection in a float zone, the exact amount of reduction achieved has not been measured or documented. Thus, for all cases, the Marangoni number was arbitrarily taken to be -1. As in the nonencapsulated zone computations, steady-state results of pure Ma convection calculations were used as initial conditions (reference cases), except for $Pr = 60$, where the reference case computations also included the quasisteady residual force $\bar{g}$. The computations were checked for the adequacy of spatial and temporal discretizations and were typically carried out over five cycles of the g-jitter frequency. Up to 56-104 time steps per cycle were utilized, and the convergence criteria of 10^{-4} was used per time step for the sum of the normalized residuals. Calculations for the lowest frequency considered in the study were the most time-consuming with a typical run consuming up to an hour of CPU time on the Cray XMP.

Silicone Oil ($Pr = 60$)

The steady-state (reference case) results show that the thermal buoyancy-driven flow (due to g) overcomes the Marangoni convection on the lower free surface of the zone and a single clockwise (CW) rotating cell occupies the entire zone. The isotherms echo the flowfield, being drawn from the hot to the cold disk along the top free surface and drawn in the opposite direction at the lower free surface. The Nu_o for this case is 1.466 as compared to 1.0 for pure conduction. The maximum velocity at the free surface is now 0.0116 mm/s, as compared to 4.43 cm/s for the unencapsulated float zone ($Ma = -10^5$).

Progressing from this starting condition, a sinusoidal disturbance with amplitude $10^{-3} g_o$ and $\omega = 10^{-3}$ Hz (case 1) is applied. A sample of the stream function and isotherm distributions over one complete cycle of the g-jitter is shown in

Table 2 Encapsulated float zones (cases simulated and inferred results)

Case no.	Fluid	$\bar{g}$, g_o	A,B, g_o	ω, Hz	$\frac{Nu_{max} - Nu_o}{Nu_o}$ %	ΔT_{max}, K	$\lvert u_{max} \rvert$, cm/s
1	Silicone oil	10^{-5}	10^{-3}	10^{-3}	281.65	20.890	78.12
2				10^{-2}	124.83	9.472	30.94
3				10^{-1}	7.75	1.110	13.36
4	1-s impulse		10^{-3}		2.58	0.569	9.002
5	1-s impulse		10^{-2}		31.32	5.120	81.48
6	Methanol	10^{-5}	10^{-3}	10^{-3}	41.51	2.71	0.845
7				10^{-2}	11.54	1.29	1.010
8				10^{-1}	1.406	0.043	0.467
9				1	0.149	0.0003	0.083
10	1-s impulse		10^{-3}		0.229	0.003	0.303
11	1-s impulse		10^{-2}		3.988	0.0221	2.819
12	Si melt	10^{-5}	10^{-3}	10^{-3}	1.10	1.725	0.0567
13				10^{-2}	0.35	0.890	0.0352
14				10^{-1}	0.03	0.119	0.0133
15	1-s impulse		10^{-3}		0.02	0.0625	0.0111
16	1-s impulse		10^{-2}		0.19	0.5650	0.0300

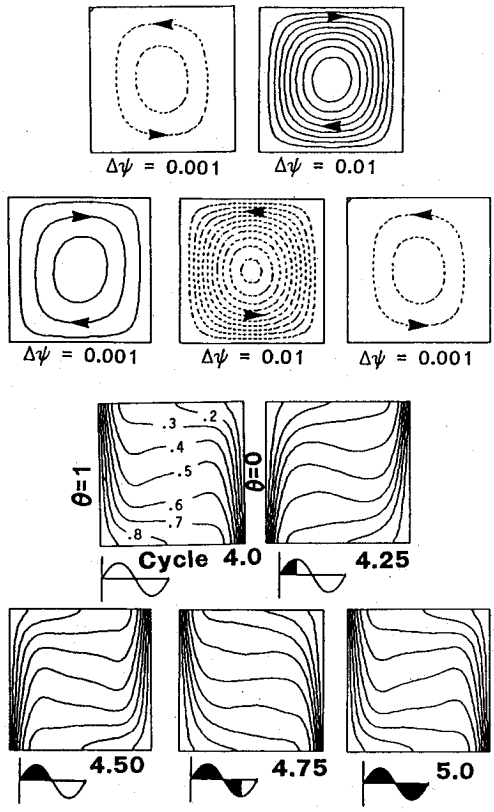

Fig. 5 Stream function and isotherm distributions: $\omega = 10^{-3}$ Hz, $Pr = 60$, $Ma = -1$.

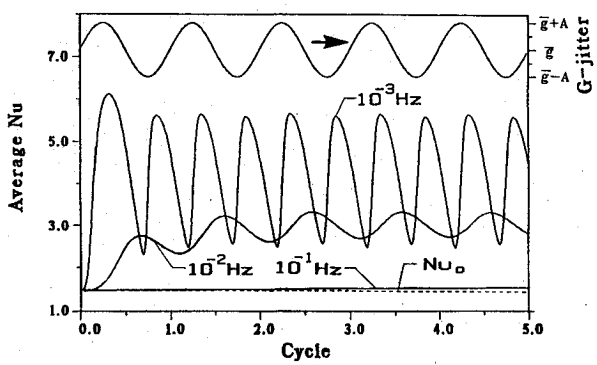

Fig. 6 Nusselt number variation due to g-jitter: $Pr = 60$, $Ma = -1$.

Figs. 5. The period of the time-varying disturbance is 1000 s for this case, which is of the same order as the orbital period (≈ 90 min) of a spacecraft around the earth. The plots are over the fourth cycle of g-jitter and are representative of the periodic behavior attained by the fluid. The stream function increments used in plotting are also listed in the figures along with the variation of g-jitter for each subplot. Specific inferences from the figures are the following.

1) The flow exhibits complete reversal over one period, although the fluid inertia causes a slight lag in the velocity response of the float zone.

2) A single cellular flow behavior is seen over a period of g-jitter.

3) The isotherms are in step with the flow field being drawn one way during the positive period of g-jitter and in the opposite direction during the negative half of the g-jitter cycle. In spite of the high Pr of the fluid (low conductivity), the isotherms show shape changes from concave to convex and vice versa due to the extremely low frequency considered.

4) The isotherm distributions suggest a rise and fall in the heat transfer rate and significant variations in the temperature at monitoring points within the zone.

The Nu variation over the five cycles of g-jitter is plotted in Fig. 6. Included in the figure are results for the other frequencies (cases 2 and 3), Nu_o, and a representation of the g-jitter variation. The plot shows an initial adjustment phase with some overshoot in Nu, but a periodic behavior is attained after one cycle of g-jitter. The maximum Nu is 5.595, a 281.6% increase over the reference case. Table 2 includes the maximum percent Nu increases over the corresponding Nu_o value for each of the cases that were calculated. For $\omega = 10^{-3}$ Hz, even the minimum Nu value of 2.564 is 74.9% larger than Nu_o. This heat transfer augmentation is also evident for all of the other frequencies, as will be discussed later. The maximum velocity at the fluid free surface is around 78 cm/s as compared to 0.0116 mm/s for the float zone with no varying g effects. This significant velocity enhancement will undoubtedly affect the distribution of solute (dopant) in the float zone. The stability and shape of the zone are other factors that will also be affected by the increased flow inside the zone. Stream function and temperature variations at specific monitoring locations (inset of figure) in the zone are presented in Fig. 7. The stream function value at the zone center ψ_B is representative of the maximum circulation strength (single cell behavior), and the plot clearly shows the complete flow reversals during the negative g-jitter cycle. It is interesting to note that the maximum and minimum ψ_B values are almost equal and, hence, the residual gravity effect is relatively small. The ψ_A and ψ_C values are equal and follow the same trend as ψ_B, but have smaller magnitudes because points A and C are located off center and the stream function has the maximum value at the cell center (one cell behavior). The temperature variations near the hot and cold walls show ripple effects but no such changes are seen at location 2 (the zone center). The crystal solidification front is located near the cold disk, and the temperature monitoring stations 3, 4, and 5 show the temperature modulation due to g-jitter at these points. Maximum temperature variations (obtained by multiplying the value of θ by ΔT) of up to 4.8 K are noticed at these stations. The low-frequency g-jitter will, thus, have a significant impact on the shape of the crystal interface. It is to be pointed out that only silicone oil, which is widely used for flow simulation purposes, displays such a drastic temperature response. Hence, the inferences drawn from results for this Pr cannot be extrapolated to a realistic melt. However, it is evident that significant flow and thermal field effects will be felt in silicone oil liquid zones, particularly at the lower end of the frequency spectrum.

Calculations for $\omega = 10^{-2}$ Hz over five cycles show similar effects as the 10^{-3}-Hz case. The isotherms display a more subdued response than the flowfield and do not show a complete change of shape as in the previous case. These small shape distortions in the time-varying isotherms also result in a sinusoidal Nu variation (Fig. 6). A lag of $\pi/2$ is observed between the g-jitter frequency and the Nu variation, unlike the previous case where the thermal phase lag is almost negligible. The thermal field takes approximately two cycles (200 s) to attain a periodic behavior, and the maximum Nu value calculated is about 125% larger than the Nu_o value. The maximum u velocity at the free surface is $\simeq 31$ cm/s, which is a 60% reduction from the 78 cm/s calculated for $\omega = 10^{-3}$ Hz. Hence, even though 10^{-2} Hz is a fairly small frequency, significant differences are seen in the fluid response to the same g-jitter amplitude of $10^{-3} g_o$ but different frequencies of 10^{-3} and 10^{-2} Hz. A combination of these two frequencies (if one follows the superposition rule) can thus result in a heat transfer augmentation in excess of 300% beyond that of the reference case. The g-jitter calculations illustrate that large, encapsulated silicone oil zones, typically used to discern fluid flow are extremely susceptible to g variations of low frequency. Such low frequencies are difficult to isolate by either

passive or active vibration isolation devices. It should be noted that encapsulation of silicone oil may not be realized in many situations. Results also suggest that silicone oil model experiments, though perhaps convenient to set up and execute, will yield results of only marginal value for application to realistic crystal growth fluids and melts.

Calculations for $\omega = 10^{-1}$ Hz (case 3) were performed over 10 cycles and significantly diminished g-jitter effects were apparent. The Nu enhancement is an order of magnitude smaller than the two previous cases, but still shows modulation due to g-jitter. This behavior, however, is not readily evident in Fig. 6 due to the scales used in the plot.

Thermal Sensitivity

In order to compare the system thermal characteristics, a thermal sensitivity parameter was defined similar to the one used in Ref. 17. It is defined as the maximum temperature difference between the g-jitter and the steady-state cases, with the comparisons always being made between points at identical locations within the zone. It is to be noted that this maximum could occur at any point inside the zone and is expressed as ΔT_{max}. This parameter gives a good measure of the thermal sensitivity of the configuration to prescribed oscillatory and impulse-type disturbances. The maximum value of this thermal sensitivity parameter determined after a periodic behavior is established is also included in Table 2 for the different cases that were computed. Specifically, Fig. 8 shows the temperature sensitivity curves for the computed frequencies over five cycles for $Pr = 60$. The figure illustrates that the lowest frequency imposed is the most sensitive. The sensitivity level is also shown to decrease as the frequency is increased. For $\omega = 10^{-3}$ Hz, the maximum temperature difference between g-jitter and the steady-state case is $\simeq 20$ K, whereas for 10^{-1} Hz, this maximum temperature drops to about 1 K. A change of up to 20 K in a zone where the system temperature difference is 32 K represents a 63% change in temperature. Such large fluctuations would result in disaster for many crystal

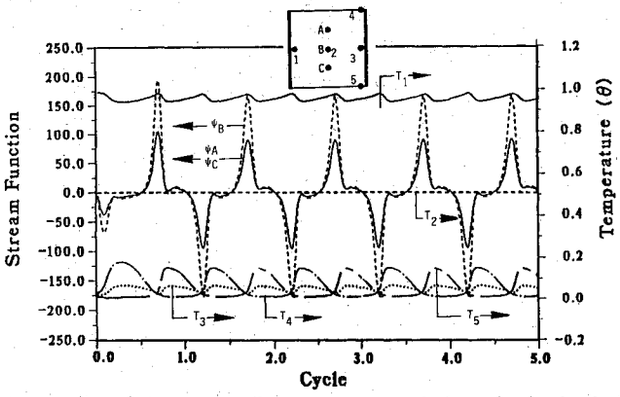

Fig. 7 Stream function and temperature variations at monitoring stations: $\omega = 10^{-3}$ Hz, $Pr = 60$, $Ma = -1$.

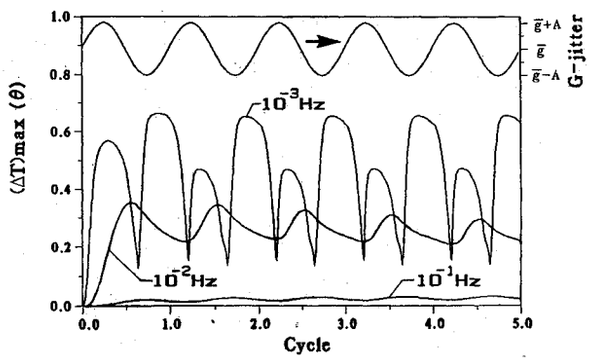

Fig. 8 Temperature sensitivity curves: $Pr = 60$, $Ma = -1$.

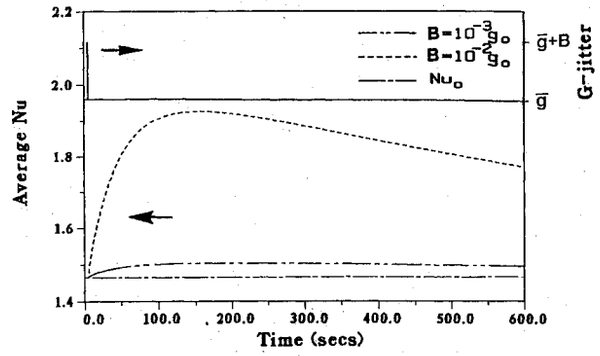

Fig. 9 Nu variation due to impulse disturbances: $Pr = 60$, $Ma = -1$.

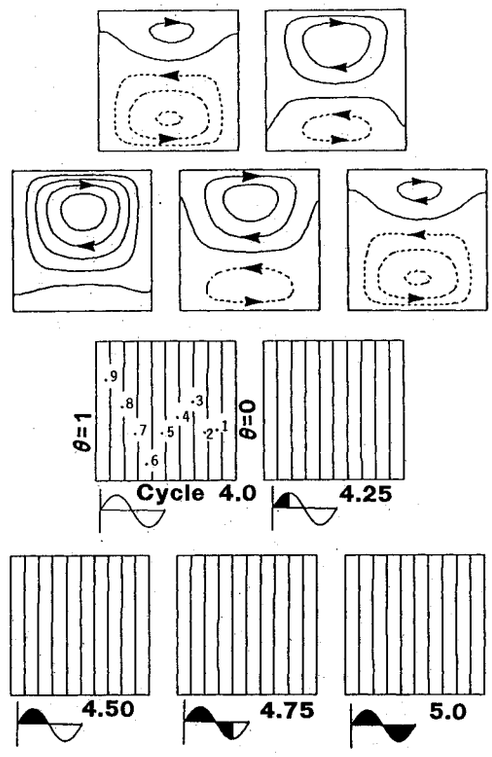

Fig. 10 Stream function and isotherm distributions: $\omega = 10^{-1}$ Hz, $Pr = 0.023$, $Ma = -1$, $\Delta\psi = 0.005$.

growth experiments. The solute distribution in a melt whose transport coefficient (Schmidt number) is large will experience similar high levels of distortion that can lead to severe crystal inhomogeneities.

Impulse Disturbances

Bridgman configuration crystal growth studies by Alexander et al.[18] have shown that impulse-type disturbances can severely affect the dopant distribution in a melt. Such impulse effects may take as long as 1000 s to completely decay and return back to flow conditions prior to the impulse. In this investigation, two disturbances were examined (cases 4 and 5 in Table 2). The impulses were of strengths 10^{-3} and $10^{-2}g_o$, respectively, and acted on the system for a period of 1 s. The background g level was maintained $10^{-5}g_o$ for both of the cases. In the calculations, the impulse was initiated at $t = 5$ s, terminated at $t = 6$ s, and the computations continued until $t = 600$ s. Approximately 1500 time steps were taken during the entire calculation. Figure 9 shows the average Nusselt number behavior over 600 s for impulses of 10^{-3} and $10^{-2}g_o$. The fluid responds to the impulse and the maximum value for Nu is reached within 2 min after the impulse was triggered.

The subsequent decay of the thermal field is a very slow process with only a 6.5% reduction from the maximum Nu value reached after 600 s of computations (case 5). The thermal diffusion time scale (L^2/α) for silicone oil is very large ($\simeq$ 12 h), and the decay of the thermal effects to the reference state can indeed take a very long time. If one extrapolates the linear decay rate seen in Fig. 9 for the $10^{-2}g_o$ impulse, a decay time of about 25 min is predicted. This faster decay rate in comparison to the slow thermal diffusion process is due to the definite but feeble convection in the zone due to the thermal buoyancy-driven flow induced by the residual g-level and the Marangoni convection. The calculated temperature changes (reference vs. impulse) for cases 5 and 4 are 5 and 0.6 K, respectively, and the maximum induced velocities due to the two impulses are 81.5 and 9 cm/s. The decay time for velocity ($\simeq$ 100 s) is much faster than the thermal field decay rate for both of the cases. It may be noted that the induced velocity of 81.5 cm/s for the $10^{-2}g_o$ impulse is about the same value as due to a g-jitter of frequency 10^{-3} Hz with an amplitude of $10^{-3}g_o$.

Similar calculations for methanol were completed, and pertinent quantities are reported in Table 2. Detailed discussion is not contained here for brevity.

Silicon Melt ($Pr = 0.023$)

Two symmetric circulation cells and no isotherm distortions are observed for the steady-state response of the melt due to $Ma = -1$. The calculated average Nusselt number is 1.00, which indicates no effect of convection on the thermal field. For a low Pr melt such as this one, the temperature field is diffusion dominated due to the high thermal conductivity, but the presence of a sufficiently strong circulation can affect the isotherm distribution as in the unencapsulated case. In this case, the effect of melt encapsulation has reduced the maximum system velocity to $\simeq$ 0.0088 cm/s compared to 145.4 cm/s for the unencapsulated case.

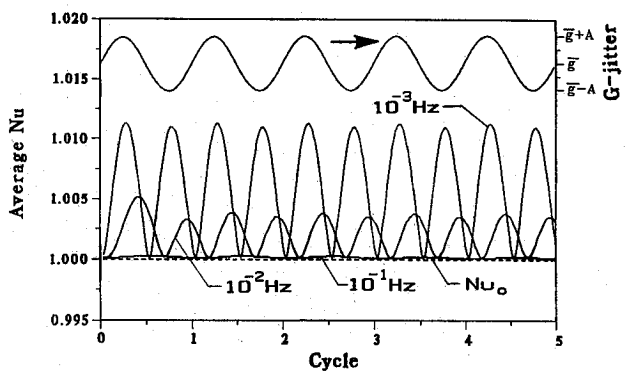

Fig. 11 Nusselt number variation due to g-jitter: $Pr = 0.023$, $Ma = -1$.

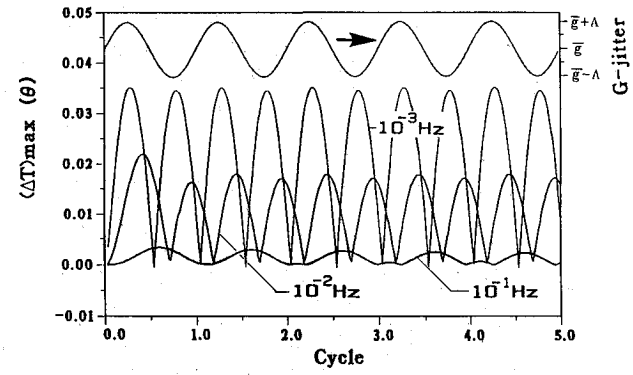

Fig. 12 Temperature sensitivity curves: $Pr = 0.023$, $Ma = -1$.

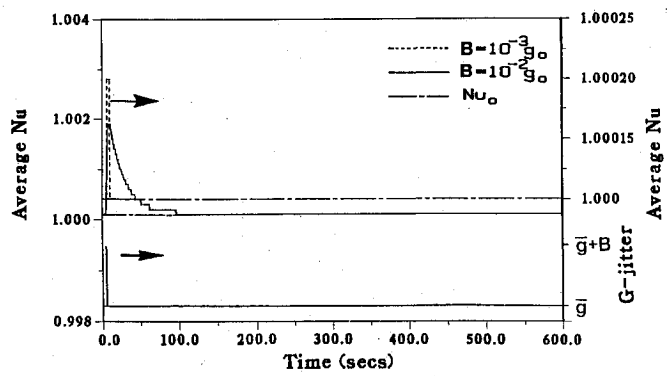

Fig. 13 Nu variation due to impulse disturbances: $Pr = 0.023$, $Ma = -1$.

The stream function and isotherms for $\omega = 10^{-1}$ Hz (case 14) are portrayed in Figs. 10 over the fourth cycle of g-jitter. The figures illustrate that g-jitter modifies the flowfield by driving the upper cell during the first half of the cycle and then driving the lower cell during the other half before reverting to a somewhat symmetrical situation at the end of the cycle. The temperature field, on the other hand, shows no effect of g-jitter or the surface tension forces. This kind of behavior of the flowfield will be of influence to the dopant distribution in a two-component melt. Semiconductor melts are frequently doped with other elements to obtain certain crystal properties, and the transport of these dopants ($Sc \simeq 10$) will be influenced by the flowfield. The oscillatory flow behavior will thus affect the solutal convection and, subsequently, the crystal composition. The low-frequency (10^{-3} and 10^{-2} Hz) flow response is essentially dominated by a single cellular flow behavior. Complete flow reversals occur in a cycle of g-jitter. The isotherm distributions for 10^{-3} Hz show some distortions and shape change, but for higher frequencies ($\omega > 10^{-3}$ Hz), the isotherms show negligible effects of g-jitter.

Average Nusselt number and temperature sensitivity plots for this Pr are presented in Figs. 11 and 12, respectively. The Nu distribution for 10^{-3} Hz shows an oscillating behavior with no phase lag occurring at the onset of computations with two Nu peaks (1.1% of Nu_o) per cycle of g-jitter. The temperature sensitivity for this frequency is 1.73 K, which is smaller than 21 K for $Pr = 60$ and 2.7 K for methanol. The silicon melt is therefore the least sensitive to g-jitter disturbances. For $\omega = 10^{-2}$ Hz, a phase lag of about $\pi/2$ is noticed between Nu and the g-jitter frequency, and some overshoot is evident in the startup period. The thermal sensitivity plot (Fig. 12) reflects the Nu plot with peak oscillations of 1.73 K for 10^{-3} Hz, 0.89 K for 10^{-2} Hz, and 0.119 K for 10^{-1} Hz. For 10^{-1} Hz, the peaks are lower by an order of magnitude but the periodic behavior is still present. The impulse disturbance responses are depicted in Fig. 13, and the plots show fairly short settling times. The thermal diffusion time scale is around 30 s.

Conclusions

The effect of g-jitter on unencapsulated and encapsulated liquid bridges was investigated. Fluid characteristics and parameters from three different experiments were employed in the calculations: a silicone oil bridge (Spacelab D1, $Pr = 60$), a methanol bridge (TEXUS 7, $Pr = 6.827$), and a silicon melt (Spacelab 1, $Pr = 0.023$). Detailed numerical modeling of unencapsulated floating zone systems was carried out. The gravity input consisted of both a steady and oscillatory acceleration component. Detailed results on the fluid flow and thermal fields were obtained. Based on these results, the following conclusions can be made.

1) The unencapsulated liquid bridges and float zone melts considered within this study were dominated by surface-ten-

sion-driven convection. Residual and g-jitter accelerations had very little impact on the flows.

2) In the steady-state computations (the reference case), maximum free surface velocities, often found near the cold wall, were very high (the highest being 145.4 cm/s for the silicon melt). Such velocities could possibly contribute to eventual oscillatory Marangoni driven convection and other detrimental effects in the actual three-dimensional experimental situation. Average surface velocities were found to be much smaller, although still significant especially for the silicon melt (8.32 cm/s). Strong fluid circulations resulted in significant distortion of the isotherms. Large values of average Nusselt numbers indicated enhanced heat transfer.

3) Transient g-jitter computations indicated that silicone oil was the most sensitive to imposed residual and sinusoidal accelerations. However, the effects were minor as compared to the Marangoni driven flows.

4) Because silicone oil will be dominated by surface-tension-driven flow and is the most sensitive to gravity disturbances, it may not be the best choice of fluids for simulation of crystal growth floating zones.

5) Because of overwhelming effects of surface tension, encapsulation may be required if striation-free float zone crystal growth is to be achieved.

Encapsulated float zones were computationally subjected to residual, oscillatory, and impulse-type disturbances. A Marangoni number, $Ma = -1$, was chosen for the calculations. Based on resultant fluid and temperature fields, the following conclusions are made.

1) Steady-state computations revealed that zone encapsulation resulted in a sizeable drop in the maximum fluid velocities. For example, for silicone oil the maximum velocity at the free surface was 0.0116 mm/s as compared to 4.43 cm/s for the unencapsulated zone. Further, the buoyancy-driven flow due to g_o overcame the Marangoni convection in the silicone oil zone, resulting in a single cell occupying the entire zone. The average Nusselt number was 1.466 (compared to 1.0 for pure conduction).

2) The g-jitter computations on the encapsulated float zones resulted in significant augmentation of the maximum velocities and heat transfer. Temperature modulation due to g-jitter was also observed along the cold wall.

3) Further, the transient computations indicated that the liquid zones have a drastic dependence on the imposed gravitational disturbances. The effects are particularly severe at the lower end of the frequency spectrum. Again, silicone oil is more sensitive to the time-varying disturbances than the other two liquids. Low-frequency accelerations will be difficult to isolate by either active or passive means.

4) Impulse disturbances were found to induce significant changes in the flow and thermal fields for all Prandtl numbers. In general, decay times to return to initial conditions were smaller than the purely diffusion time scale.

5) The silicon melt was least sensitive to g-jitter accelerations. Zone encapsulation reduces the maximum free surface velocity from 145.4 cm/s (unencapsulated case) to 0.0088 cm/s. When residual and sinusoidal accelerations are imposed, the temperature field shows no effect, although g-jitter modifies the flowfield. Thus, encapsulation of the silicon melt appears to be an attractive space processing option. However, oscillatory behavior of the fluid flow will tend to affect the solutal convection and subsequent crystal composition. Impulse disturbances were found to have a decay time comparable to the thermal diffusion time scale.

Acknowledgment

This work was supported under the Advanced Technology Development Vibration Isolation initiative sponsored by NASA Headquarters, Microgravity Science and Applications Division.

References

[1]Eyer, A., Leiste, H., and Nitsche, R., "Crystal Growth of Silicon in Spacelab-1: Experiment ES-321," *Proceedings of the 5th European Symposium on Material Sciences Under Microgravity* (Schloss Elmau, Germany), European Space Agency, Paper SP-222, Paris, Nov. 1984, pp. 173–182.

[2]Eyer, A., and Leiste, H., "Striation-Free Silicon Crystals by Float-Zoning with Surface Coated Melt," *Journal of Crystal Growth,* Vol. 71, 1985, pp. 249–252.

[3]Croell, A., Mueller, W., and Nitsche, R., "Growth of a SiO_2 Coated Silicon Crystal," *TEXUS 11/12 Abschlussbericht,* edited by H. Alborn, BMFT/DFVLR, Germany, 1985 (in German).

[4]Croell, A., Mueller, W., and Nitsche, R., "Dopant Distribution in Semiconductor Crystals Under Microgravity," *6th European Symposium on Material Sciences Under Microgravity Conditions,* European Space Agency, Paper SP-256, Paris, 1986, pp. 87–94.

[5]Barocela, E., and Jalilevand, A., "Liquid Encapsulated Float Zone Method for Microgravity Production of Gallium Arsenide," AIAA Paper 87-0390, Reno, NV, Jan. 1987.

[6]Ostrach, S., "Low Gravity Fluid Flows," *Annual Review of Fluid Mechanics,* Vol. 14, 1982, pp. 313–345.

[7]Demel, K., "Implications of Acceleration Environments on Scaling Materials Processing in Space to Production," *Workshop Proceedings of Measurement and Characterization of the Acceleration Environment on Board the Space Station,* Teledyne Brown Engineering, Huntsville, AL, Aug. 1986.

[8]Hammacher, H., "Simulation of Weightlessness," *Materials Sciences in Space,* edited by B. Feurbacher, H. Hammacher, and R. J. Naumann, Springer-Verlag, Heidelberg, Germany, 1986, pp. 31–52.

[9]Martinez, I., and Meseguer, J., "Floating Liquid Zones in Microgravity," *Scientific Results of the German Spacelab Mission—D1* (Abstracts of the D1 Symposium, Norderney, Germany), Wissenschaftliche Projektfuhrung D1, DFVLR, Germany, Aug. 1986, pp. 31,32.

[10]Da Riva, I., and Martinez, I., "Floating Liquid Zones," *Natur Wissenschaften,* Vol. 73, 1986, pp. 345–347.

[11]Winter, C. A., "A Database Documenting Fluids and Materials Processing Experiments Performed in Space," AIAA Paper 89-0864, Reno, NV, Jan. 1989.

[12]Napolitano, L. G., Monti, R., and Russo, G., "Marangoni Convection in One and Two Liquid Floating Zones," *Natur Wissenschaften,* Vol. 73, 1986, pp. 352–355.

[13]Chun, Ch.-H., "Verification of Turbulence Developing from the Oscillatory Marangoni Convection in a Liquid Column," *Proceedings of the 5th European Symposium on Material Sciences Under Microgravity* (Schloss Elmau, Germany) European Space Agency, Paper ESA SP-222, Paris, Nov. 1984, pp. 271–280.

[14]Gosman, A. D., Pun, W. M., Runchal, A. K., Spalding, D. B., and Wolfshtein, M., *Heat Transfer in Recirculating Flows,* Academic Press, New York, 1969.

[15]Van Doormal, J. P., and Raithby, G. D., "Enhancements of the SIMPLE Method for Predicting Incompressible Fluid Flows," *Numerical Heat Transfer,* Vol. 8, 1985, pp. 635–652.

[16]Latimer, B. R., and Pollard, A., "Comparison of Pressure-Velocity Coupling Solution Algorithms," *Numerical Heat Transfer,* Vol. 8, 1985, pp. 635–652.

[17]Spradley, L. W., Bourgeois, S. V., and Lin, F. N., "Space Processing Convection Evaluation: G-Jitter Convection in Confined Fluids in Low Gravity," AIAA Paper 75-695, Jan. 1975.

[18]Alexander, J. I. D., Ouazzani, J., and Rosenberger, F., "Analysis of Low Gravity Tolerance of Bridgeman-Stockbarger Crystal Growth I: Steady and Impulse-Type Accelerations," *Journal of Crystal Growth,* Vol. 97, 1989, pp. 285–302.

Alfred L. Vampola
Associate Editor